Factors affecting the rare earth element compositions in massive sulfides from deep-sea hydrothermal systems

Zhigang Zeng[1,2], Yao Ma[1,3], Xuebo Yin[1], David Selby[4], Fancui Kong[1], and Shuai Chen[1]

[1]Seafloor Hydrothermal Activity Laboratory of the Key Laboratory of Marine Geology and Environment, Institute of Oceanology, Chinese Academy of Sciences, Qingdao, China, [2]Qingdao Collaborative Innovation Center of Marine Science and Technology, Qingdao, China, [3]College of Earth Science, University of Chinese Academy of Sciences, Beijing, China, [4]Department of Earth Sciences, University of Durham, Durham, UK

Abstract To reconstruct the evolution of ore-forming fluids and determine the physicochemical conditions of deposition associated with seafloor massive sulfides, we must better understand the sources of rare earth elements (REEs), the factors that affect the REE abundance in the sulfides, and the REE flux from hydrothermal fluids to the sulfides. Here we examine the REE profiles of 46 massive sulfide samples collected from seven seafloor hydrothermal systems. These profiles feature variable total REE concentrations (37.2–4092 ppb) and REE distribution patterns (La_{CN}/Lu_{CN} ratios = 2.00–73.8; $(Eu/Eu^*)_{CN}$ ratios = 0.34–7.60). The majority of the REE distribution patterns in the sulfides are similar to those of vent fluids, with the sulfides also exhibiting light REE enrichment. We demonstrate that the variable REE concentrations, Eu anomalies, and fractionation between light REEs and heavy REEs in the sulfides exhibit a relationship with the REE properties of the sulfide-forming fluids and the massive sulfide chemistry. Based on the sulfide REE data, we estimate that modern seafloor sulfide deposits contain approximately 280 t of REEs. According to the flux of hydrothermal fluids at mid-ocean ridges (MORs) and an average REE concentration of 3 ng/g in these fluids, hydrothermal vents at MORs alone transport more REEs (>360 t) to the oceans over the course of just 2 years than the total quantity of REEs in seafloor sulfides. The excess REEs (i.e., the quantity not captured by massive sulfides) may be transported away from the systems and become bound in sulfate deposits and metalliferous sediments.

1. Introduction

The chemical properties of rare earth elements (REEs) in a trivalent state under most natural conditions are fundamentally similar [*Henderson*, 1984], but slight differences in their behavior are caused by the decrease in atomic radii across the group, which influences fractionation, complexation, adsorption, speciation, and mobility [*Henderson*, 1984; *Elderfield et al.*, 1988]. The study of REEs in seafloor hydrothermal systems is key to evaluate the sources of fluid constituents, mixing processes, and fluid evolution [*Alt*, 1988; *Elderfield et al.*, 1988; *Gillis et al.*, 1990; *Haas et al.*, 1995; *Humphris*, 1998; *Humphris and Bach*, 2005; *Embley et al.*, 2007; *Zeng et al.*, 2009]. In addition, REE data may be used to evaluate the physicochemical conditions of hydrothermal fluids [*Michard et al.*, 1983; *Michard and Albarède*, 1986; *Michard*, 1989; *Klinkhammer et al.*, 1994; *James et al.*, 1995; *Douville et al.*, 1999; *Bach et al.*, 2003; *Mills and Elderfield*, 1995]. As such, REE data provide important information about (1) the geochemical nature of ancient hydrothermal activity [*Rimskaya-Korsakova and Dubinin*, 2003; *Schmidt et al.*, 2010; *Cole et al.*, 2014]; (2) the impact of hydrothermal activity on the chemical mass balance of elements between sulfides and seawater [*German et al.*, 1990; *Mitra et al.*, 1994; *Bau and Dulski*, 1999; *Sherrell et al.*, 1999]; (3) magmatic degassing in seafloor hydrothermal systems [*Craddock et al.*, 2010]; and (4) the formation conditions and sources of seafloor sulfides, sulfates, and native sulfur balls and chimneys [e.g., *Graf*, 1977; *Alt*, 1988; *Barrett et al.*, 1990; *Gillis et al.*, 1990; *Mills and Elderfield*, 1995; *Bach et al.*, 2003; *Rimskaya-Korsakova and Dubinin*, 2003; *Zeng et al.*, 2007, 2009, 2010, 2011].

The majority of seafloor hydrothermal fluids have REE concentrations that are several orders of magnitude higher than those of seawater [*Turekian*, 1968]. Seafloor hydrothermal fluids have remarkably uniform REE distribution patterns, exhibiting greater enrichment in light REEs (LREEs) than heavy REEs (HREEs), and positive Eu anomalies [e.g., *Michard and Albarède*, 1986; *Michard*, 1989; *Klinkhammer et al.*, 1994; *Mitra et al.*, 1994; *Douville et al.*, 1999]. However, in some hydrothermal systems (e.g., the Comfortless Cove vent field,

Mid-Atlantic Ridge (MAR) near 5°S and the East Scotia subduction zone located in the Atlantic sector of the Southern Ocean), the hydrothermal fluids have extremely high REE concentrations (up to 123 nmol/kg), are enriched with mid-REEs (MREEs), and have negative Eu anomalies due to the accumulation of particulate anhydrite, which is MREE enriched and sourced from black and white chimneys [*Schmidt et al.*, 2010; *Cole et al.*, 2014]. In the Manus Basin, the REE patterns in different vent fluids range from LREE enriched, to MREE and HREE enriched, to flat, and show positive Eu anomalies due to the differences in the degassing of magmatic volatiles (i.e., HF and SO_2) and the precipitation of anhydrite in submarine hydrothermal systems [*Craddock et al.*, 2010]. The different REE patterns in the hydrothermal fluids are mainly attributed to differences in REE solubility due to variations in the relative abundance and stability of REE-chloride, fluoride, and sulfate complexes as a function of fluid temperature, pH, and ligand concentration [*Craddock et al.*, 2010].

To date, limited data are available on the REE compositions of sulfides from various deep-sea hydrothermal systems in mid-ocean ridges (MORs) and back-arc basins (BABs), due to the difficulty in obtaining pure sulfide mineral or aggregate samples that exclude other minerals such as sulfates and oxides [*Graf*, 1977; *Barrett et al.*, 1990; *Mills and Elderfield*, 1995]. However, the range of REE concentrations in the sulfide minerals (10–100,000 ppb) [*Graf*, 1977; [*Gillis et al.*, 1990; *Mills and Elderfield*, 1995; *Zeng et al.*, 2010] encompasses the REE concentrations in the oceanic crust (~57 ppm) [*Hofmann*, 1988] and vent fluids (<33 ppb) [*Michard and Albarède*, 1986; *Michard*, 1989; *Klinkhammer et al.*, 1994; *Mitra et al.*, 1994; *James et al.*, 1995; *Bau and Dulski*, 1999; *Douville et al.*, 1999, 2002; *Schmidt et al.*, 2007]. The REE patterns are variable in hydrothermal sulfides. For example, the massive sulfide-sulfates in the Southern Explorer Ridge exhibit three REE patterns: (1) enrichment in LREEs with positive Eu anomalies, (2) flat REE patterns with positive Eu anomalies and negative Ce anomalies, and (3) enrichment in LREEs with moderately negative Ce anomalies [*Barrett et al.*, 1990]. The varying sulfide-sulfate REE patterns are interpreted as the result of variable mixtures of hydrothermal fluids and seawater [*Barrett et al.*, 1990]. In the Rainbow, Broken Spur, and Trans-Atlantic Geotraverse (TAG) hydrothermal fields, the chondrite-normalized REE patterns of 10 seafloor hydrothermal sulfide samples display enrichment in LREEs relative to HREEs, which has been attributed to crystallographic control [*Mills and Elderfield*, 1995; *Rimskaya-Korsakova and Dubinin*, 2003]. The REE patterns of the massive sulfides in the Rainbow field and Southern Explorer Ridge exhibit positive Eu anomalies, but those in the TAG, Broken Spur, and Snake Pit field feature negative Eu anomalies [*Barrett et al.*, 1990; *Gillis et al.*, 1990; *Rimskaya-Korsakova and Dubinin*, 2003]. The variability in the Eu anomalies may be related to the temperature (from <200 to >300°C) of sulfide precipitation in these seafloor hydrothermal systems [*Mills and Elderfield*, 1995].

In this study, we analyzed the REE compositions of 46 seafloor massive sulfide samples from seven hydrothermal fields associated with the MAR, East Pacific Rise (EPR), Central Indian Ridge (CIR), Southwest Indian Ridge (SWIR), and North Fiji basin (NFB). The REE compositions of the massive sulfides from these seafloor hydrothermal systems are presented in combination with the major and trace element compositions to (1) identify the sources of the REEs in sulfides, (2) understand the factors that cause variations in the REE distribution patterns in sulfides, and (3) evaluate the flux of REEs from hydrothermal fluids to seafloor massive sulfides.

2. Geological Setting and Sample Mineralogical Descriptions

Sulfide samples were recovered by TV-grab samplers from the fast spreading EPR near 13°N, the ultrafast spreading EPR near 1°S–2°S, the Kairei hydrothermal field (KHF) and the Edmond hydrothermal field (EHF) on the intermediate spreading CIR near 25°S, the "A" area of the ultraslow spreading SWIR, and the Logatchev hydrothermal field (LHF) on the slow spreading MAR near 15°N in 2005 and 2008 during the DY105-17 and DY115-20 cruises of the R/V *Dayang Yihao*. Sulfide samples from the Sonne 99 hydrothermal field (S99HF) in the back-arc NFB were collected in 1998 during the SO134 cruise of HYFIFLUX II (Figure 1 and Table 1).

The massive sulfide deposits of the EPR near 13°N and 1°S–2°S, EHF, and the "A" area are hosted by mid-ocean ridge basalts (MORBs) [*Zeng et al.*, 2014]. In the KHF, the massive sulfide deposit is hosted by basalt that is adjacent to mafic-ultramafic olivine-rich rocks [*Kumagai et al.*, 2008], and the hydrothermal fluids interact with and circulate through ultramafic rocks [*Nakamura et al.*, 2009]. In the LHF, the massive sulfide is associated with ultramafic rocks in a debris flow that consists of heterogeneous ultramafic and mafic intrusive rocks, including serpentinized harzburgite, serpentinized dunite, gabbronorite, and olivine-bearing
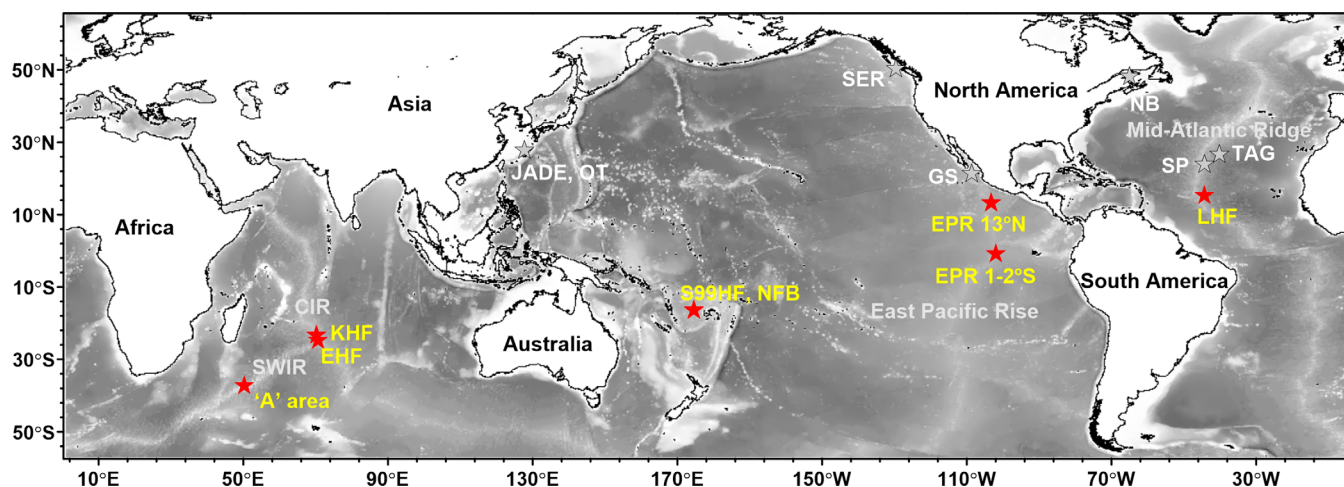
Figure 1. Locations of the seafloor massive sulfide samples from deep-sea hydrothermal fields. The red stars indicate the seven sulfide sample sites from the East Pacific Rise (EPR) near 13°N and 1°S–2°S, Kairei hydrothermal field (KHF) and Edmond hydrothermal field (EHF) in the Central Indian Ridge (CIR), "A" area hydrothermal field ("A" area) in the Southwest Indian Ridge (SWIR), Sonne 99 hydrothermal field (S99HF) in the North Fiji Basin (NFB), and Logatchev hydrothermal field (LHF). The gray stars indicate the sulfide sample sites from the Trans-Atlantic Geotraverse (TAG), Snake Pit (SP), New Brunswick (NB), Southern Explorer Ridge (SER), Green Seamount (GS), and JADE in the Okinawa Trough (OT).

basalt, and the area is largely covered by pelagic sediment [*Mozgova and Efimov*, 1999; *Rouxel et al.*, 2004; *Petersen et al.*, 2009]. The S99HF in the NFB is hosted by normal mid-ocean ridge basalt (N-MORB) and ocean island basalt (OIB) [*Eissen et al.*, 1994; *Nohara et al.*, 1994; *Koschinsky et al.*, 2002; *Kim et al.*, 2006]. Massive sulfide deposits include those formed from both focused high-temperature (>300°C) fluid outflow through chimneys and medium (300–200°C) to low-temperature (<200°C) fluids from mounds in the EPR (near 13°N), KHF, EHF, LHF, and NFB [*Michard et al.*, 1984; *Bowers et al.*, 1988; *Merlivat et al.*, 1987; *Ishibashi et al.*, 1994a, 1994b; *Koschinsky et al.*, 2002; *Gallant and Von Damm*, 2006; *Schmidt et al.*, 2007] (Table 2).

Tables 1 and 3 provide information on the sampling locations, depths, and mineralogy of the massive sulfide samples. The massive sulfide samples consist primarily of pyrite ± marcasite, chalcopyrite, sphalerite, anhydrite, barite, amorphous silica, and minor galena (Table 3). Four sample types were studied: Fe rich, Zn rich, Fe–Cu rich, and Si rich (Table 3).

3. Samples and Analytical Methods

3.1. Sampling Procedures

The collected samples were separated into small (<1 cm) chips according to differences in color, grain size, porosity, conduits, and concentric zones. The samples did not have a fixed shape and volume, but the primary weight of most samples ranged from 4 to 46 g, except for the samples from EPR near 13°N, which exceeded 100 g. All the sample chips were crushed with an agate mortar and pestle and sieved to select sulfide grains between 50 μm and 2 mm in size [*Zeng et al.*, 2014]. The sulfides were separated from

Table 1. Locations of the Sulfide Samples From the Seafloor Hydrothermal Systems[a]

Field	Sample Number	Latitude	Longitude	Depth (m)
13°N, EPR	EPR05-TVG1-2-1, 3, 4, 5	12°42.669′N	103°54.426′W	2628
13°N, EPR	EPR05-TVG1-3-1, 3, 4, 5, 6	12°42.669′N	103°54.426′W	2628
13°N, EPR	EPR05-TVG2-1-1, 2, 3, 4, 5, 6, 7, 8	12°42.678′N	103°54.414′W	2633
1°-2°S, EPR	20III-S4-TVG1-1-2, 3, 4	1°22.130′S	102°37.360′W	2747
KHF, CIR	IR05-TVG9-1, 2, 3	25°19.221′S	70°02.420′E	2437
EHF, CIR	IR05-TVG12-3, 8-4, 14	23°52.678′S	69°35.808′E	3293
EHF, CIR	IR05-TVG13-4-2, 9.2-1, 9.2-2	23°52.684′S	69°35.795′E	3292
"A" area, SWIR	20V-S35-TVG17-1-1, 1-2, 2, 3-2, 4-2, 5-1, 5-2, 6	37°46.812′S	49°38.886′E	2783
S99HF, NFB	26.2GTV-2	16°57.602′S	173°54.991′E	1976
S99HF, NFB	42GTV-1, 2, 3	16°57.533′S	173°54.978′E	1975
S99HF, NFB	113.1GTV-1, 2, 4	16°57.322′S	173°54.970′E	1967
S99HF, NFB	113.2GTV	16°57.322′S	173°54.970′E	1967
LHF, MAR	MAR05-TVG1-9, 10-2	14°45.186′N	44°58.772′W	3025

Table 2. Major Physicochemical Compositions of Hydrothermal Fluids in Various Seafloor Hydrothermal Systems From Different Tectonic Settings

Field	T (°C)	pH (25°C)	Cl⁻ (mmol/kg)	SO_4^{2-} (mmol/kg)	Host Rock
13°N, EPR[a]	<283–354	3.1–3.3	712–760	0	MORB
KHF, CIR[b]	315–365	3.35–3.51	571–620	0.479–1.56	MORB + mafic-ultramafic rock
EHF, CIR[b]	273–382	<2.97–3.13	926–933	0–0.615	MORB
HBS, diffuse fluid, NFB[c]	11.29–12.46	6.98–7.35	552–555	-[d]	MORB + OIB
Kaiyo site, NFB[c]	291	4.7	267	-	MORB + OIB
LHF, MAR[e]	170–353	3.3–3.9	515–551	0.8–2.5	Ultramafic rock + basalt + sediment
Seawater[f]	2–4	7.8–8.1	542–560	28	

[a]Data from *Bowers et al.* [1988], *Fouquet et al.* [1988], *Merlivat et al.* [1987], and *Michard et al.* [1984].
[b]Data from *Gallant and Von Damm* [2006].
[c]Data from *Ishibashi et al.* [1994a, 1994b] and *Koschinsky et al.* [2002].
[d]"-" No data available.
[e]Data from *Koschinsky et al.* [2008].
[f]Data from *Charlou et al.* [2002], *Douville et al.* [2002], and *Gallant and Von Damm* [2006].

nonsulfide minerals, e.g., sulfates and amorphous silica, via ethanol elutriation [*Zeng et al.*, 2014]. This purification of the sulfide aliquots by ethanol elutriation is based on specific gravity and uses a stream of ethanol that flows counter to the direction of grain flow in a glass dish. The less dense particles rise to the top

Table 3. Mineralogy and Types of Sulfide Samples From Seafloor Hydrothermal Systems Based on XRD, Polarized Optical Microscopy, and SEM Analysis[a]

Field	Sample Number	Macroscopic Descriptions	Mineralogy Abundant	Mineralogy Major	Mineralogy Minor	Sample Type
13°N, EPR	EPR05-TVG1-2	Fe-rich dense massive sulfides coated with orange Fe oxides, occurrence of small conduits and well-developed crystals	Py		Cpy, Sp	Fe rich
13°N, EPR	EPR05-TVG1-3	Fe-rich massive sulfides coated with orange oxides, local occurrence of oxidized pyrite druse	Py		Cpy, Sp	Fe rich
13°N, EPR	EPR05-TVG2-1	Fe-rich massive sulfides with many oval cavities inside, occurrence of mineral zonation, and tube worm casts	Py, Mc		Sp	Fe rich
1°S–2°S, EPR	20III-S4-TVG1-1	Fragment of porous chimney with two partially filled conduits, dense exterior, locally altered to bluish purple	Py		Cpy, Mc	Fe rich
KHF, CIR	IR05-TVG9	Fragment of chimney, occurrence of finely bladed chalcopyrite	Py	Cpy	Sp	Fe–Cu rich
EHF, CIR	IR05-TVG12-3	Fragments of gray silica minerals and brown oxides with finely disseminated sulfide minerals, minor barite	Silica	Mc, Py, Sp	Ba	Si rich
EHF, CIR	IR05-TVG12-8-4	Fragment of gray-black Zn-rich porous massive sulfides coated with red to brown oxide crusts	Sp	Py, Mc, S	Cpy	Zn rich
EHF, CIR	IR05-TVG12-14	Gray-black fragment of porous massive sulfide associated with yellowish brown oxides	Sp	Py, Mc, S	Cpy	Zn rich
EHF, CIR	IR05-TVG13-4-2	Oxidized columnar chimney coated with red-brown oxides, dense without apparent zonation, two oval fluid conduits	Cpy, Mc	Sp, Py		Fe–Cu rich
EHF, CIR	IR05-TVG13-9.2	Fragment of chimney, a small columnar chimney attached, abundant red, brown, and yellowish green mixture of oxides, anhydrite, and barite	Mc, Anh	Cpy, Py, Sp, Gyp	Ba	Fe rich
"A" area, SWIR	20V-S35-TVG17	Dense massive sulfide consisting mainly of pyrite and pyrrhotite, partially oxidized interior, dark brown oxide crusts	Py	Po	Cpy, Mc, Sp	Fe rich
S99HF, NFB	26.2GTV-2	Gray zinc-rich fragment from the exterior of a chimney, local honeycomb structure, and coarse black sphalerite crystals	Sp	Mc	Cpy, Py, Gn	Zn rich
S99HF, NFB	42GTV-1	Fragment of Cu-rich chimney with several conduits inside.	Mc	Py, Cpy		Fe–Cu rich
S99HF, NFB	42GTV-2	Subsamples were taken from outside to inside	Mc, Cpy	Py		Fe–Cu rich
S99HF, NFB	42GTV-3		Mc, Cpy	Py		Fe–Cu rich
S99HF, NFB	113.1GTV-1	Fragment of porous massive sulfide, Fe-rich interior, and siliceous exterior. 113.1GTV-1 and 113.1GTV-2 were taken	Py	Cp, Mc		Fe rich
S99HF, NFB	113.1GTV-2	ceous exterior. 113.1GTV-1 and 113.1GTV-2 were taken	Py	Ma, Cp		Fe rich
S99HF, NFB	113.1GTV-4	from the interior, and 113.1GTV-4 was taken from the exterior, which consists of amorphous silica, with minor barite	Silica	Py, Cpy, Sp	Ba	Si rich
S99HF, NFB	113.2GTV	Fragment of massive sulfide, higher-porosity exterior	Py	Mc	Sp, Cpy	Fe rich
LHF, MAR	MAR05-TVG1-9	Cu-rich massive sulfide with more porous exterior, light blue secondary minerals on the surface	Cpy	Py	Sp	Fe-Cu rich
LHF, MAR	MAR05-TVG1-10-2	Cemented block of gypsum and amorphous silica, disseminated chalcopyrite and marcasite, mottled oxides outside	Cpy	Py	Mc	Fe–Cu rich

[a]Py: pyrite; Mc: marcasite; Cpy: chalcopyrite; Sp: sphalerite; Po: pyrrhotite; Silica: amorphous silica; Ba: barite; S: sulfur; Gn: galena; Anh: anhydrite; Gyp: gypsum. Abundant: >30%, major: 5–30%, and minor: <5%.

(overflow) because their terminal grain velocities are lower than the velocity of the rising fluid. Because most of the samples were fine grained and intergrown, an integrated mechanical separating method was used to obtain a pure monomineralic sulfide or mineral aggregate separate. The separation methods included a high-frequency dielectric splitter, magnetic separator, and electromagnetic separator [*Zeng et al.*, 2014]. All the elemental analysis sulfide samples were then carefully picked manually under a binocular microscope to avoid sulfates and oxides and were ultrasonically cleaned in ultrapure alcohol to remove any seawater influences, e.g., the presence of salts and altered seawater products. Then, all the samples were ground to a powder finer than 63 μm in an agate mortar [*Zeng et al.*, 2014]. Fine-grained glass powder was used as an abrasive to polish the mortar and pestle between samples to exclude cross contamination.

3.2. Analytical Methods

The sample mineralogy was determined by X-ray diffraction (XRD) (D/MAX-2400) at the Institute of Geology and Geophysics and by polarized optical microscopy at the Institute of Oceanology, Chinese Academy of Sciences. The D/MAX-2400 instrument was operated at 40 kV and 40 mA, at a scan range of $2\theta = 3°$–$65°$, a scan step of 0.02, and a scan velocity of 0.5 s/step. In addition, polished thin sections were analyzed with a TESCAN VEGA 3 LMH scanning electron microscope (SEM) to obtain qualitative analyses of sulfide, oxide, and sulfate minerals from back-scattered electron (BSE) images and energy dispersive spectrometry (EDS).

Each sample was divided into two subsamples, one for major and trace elements and one for REE abundances. The major and trace element abundances were measured on separate 40 mg splits of powdered sulfide separates. These pretreated samples were digested in vials by using 0.5 mL of 22.5 mol/L HF, 2 mL of 12 mol/L HCl, and 0.7 mL of 16 mol/L HNO$_3$ (all acids at metal-oxide-semiconductor pure grade) at 150°C for 24 h in closed Teflon vials on an electrothermal hotplate. Then, 0.2 mL of 12.4 mol/L HClO$_4$ was added, and the samples were dried at 120°C until no white smoke was present. When the samples were almost dry, 1 mL of 16 mol/L HNO$_3$ and 1 mL of deionized Milli-Q water (18.2 MΩ cm resistivity) were added, and the mixture was reheated in closed vials on the hotplate at 120°C for 12 h [*Yin et al.*, 2011]. The major elements Fe, Cu, and Zn were analyzed with an IRIS Intrepid II XSP ICP-AES (Thermo Fisher Scientific) at the Qingdao Institute of Marine Geology. The relative standard deviation (RSD), which was calculated from standard reference materials, was <2%. The trace elements were analyzed by an ICP-MS (ELAN DRC II) at the Institute of Oceanology, Chinese Academy of Sciences. The RSD was <10%. The reference materials GBW07267 (pyrite), GBW07268 (chalcopyrite), GBW07270 (sphalerite), and WMS-1a were run as external standards by using the above analytical protocols to evaluate the accuracy and precision during our measurements (Table 4).

A modified inductively coupled plasma mass spectrometer (ICP-MS) technique was developed to measure the 14 REEs and to correct for analytical interferences in Ba-rich samples. The process was performed on 100 mg of a powdered sulfide sample in a Teflon vial, into which 2 mL of 12 mol/L HCl, 0.5 mL of 22.5 mol/L HF, and 0.6 mL of 16 mol/L HNO$_3$ were added in turn. Then, the mixture of sample and acid solution was heated at 150°C for 48 h in a closed vial. The resulting solutions were clear and free of precipitates. Following digestion, the samples were dried at 120°C, and when they were almost dry, 2 mL of 2 mol/L HCl was added and heated again for 12 h in closed vials. A Chinese 732 cation-exchange resin column (a strongly acidic styrene-type cation exchange resin) was washed with 6 mL of 2 mol/L HCl before passing the dissolved samples through the column. To remove the matrix elements (e.g., Fe, Cu, Pb, Zn, and Ba), 4 mL of 2 mol/L HCl was added. To remove the Ba, 3 mL of 2.5 mol/L HNO$_3$ was added (90% recovery), along with 6 mL of 4 mol/L HNO$_3$ to elute the REEs into Teflon vials. The collected REEs were evaporated until almost dry. The samples were redissolved with 2 mL of 0.32 mol/L HNO$_3$ and diluted to 5 mL in a centrifugal tube. Finally, the REEs were analyzed with an ICP-MS (ELAN DRC II) at the Institute of Oceanology, Chinese Academy of Sciences. The efficiency of Ba removal was >90%. An isotope correction formula was applied to correct for the interference of residual Ba (<10%) on Eu: $I\ (^{151}Eu)_c = I\ (^{151}Eu)_m - (A\ (^{135}Ba)/A\ (^{134}Ba)) \times (I\ (^{149}Sm)_m - (A\ (^{149}Sm)/A\ (^{147}Sm)) \times I\ (^{147}Sm)_m)$, where $I\ (^{151}Eu)_c$ is the corrected intensity of ^{151}Eu, $I\ (^{151}Eu)_m$ is the measured intensity of ^{151}Eu, $A\ (^{135}Ba)$ is the relative abundance (6.592%) of ^{135}Ba [*Rosman and Taylor*, 1998], $A\ (^{134}Ba)$ is the relative abundance (2.417%) of ^{134}Ba [*Rosman and Taylor*, 1998], $I\ (^{149}Sm)_m$ is the measured intensity of ^{149}Sm, $A\ (^{149}Sm)$ is the relative abundance (13.8%) of ^{149}Sm [*Rosman and Taylor*, 1998], $A\ (^{147}Sm)$ is the relative abundance (15.0%) of ^{147}Sm [*Rosman and Taylor*, 1998], and $I\ (^{147}Sm)_m$ is the measured intensity of ^{147}Sm. In this formula, the unit of intensity is counts per second (CPS). Data on yttrium (Y) are not provided here because of the low recovery rate (between 45 and 60%). Using GBW07270, the

Table 4. Analyses of Standard Reference Materials[a]

Element	Blank Average	DLOM Blank + 3δ	WMS-1a				GBW07267					GBW07268				GBW07270			
			Average	Reference Value	Added (200 ng)	Mean Recovery (%)	Average	Reference Value	DVNM	Added (200 ng)	Mean Recovery (%)	Average	Reference Value	Added (200 ng)	Mean Recovery (%)	Average	Reference Value	Added (200 ng)	Mean Recovery (%)
Fe (%)	0.014	0.531	44.0	45.4 ± 0.5			40.93	46.08 ± 0.29				30.9	30.30 ± 0.28			2.41	2.14 ± 0.14		
Cu (ppm)	0.006	0.219	14,534	13,960 ± 140			391	431 ± 30				300,117	333,000 ± 1,700			1,066	1,000 ± 100		
Zn (ppm)	<0.005	0.027	160	130 ± 4			277	219 ± 17				3,093	3,000 ± 300			587,970	625,100 ± 1,700		
Al (ppm)			13,363	13,500 ± 210			605					401				50			
Ti (ppm)			801	840 ± 20			241					2.02				6.37			
Ba (ppm)			62.6	70			1.51					0.37				3.53			
La (ppb)	3.52	5.58	4,064	4,300	4,209		5,054		4,853	5,474		45.6		240	97.2	78.3		274	97.6
Ce (ppb)	6.93	9.07	7,655	7,900	7,904		10,488		10,864	11,222		92.3		274	91	204		363	89.4
Pr (ppb)	0.63	0.79	821	1,000	980		1,052		1,176	1,164		11		218	103	32.0		236	102
Nd (ppb)	2.05	2.25	3,323	4,000	3,556		4,018		4,148	4,187		40.7		250	105	159		349	94.8
Sm (ppb)	0.40	0.58	801	800	1,028	114	749		688	908		6.82		218	105	50.0		268	109
Eu (ppb)	0.15	0.26	231	200.0	437	103	106		92.0	288	90.7	1.32		209	104	13.4		236	111
Gd (ppb)	0.39	0.59	858	800	1,087	115	469		423	647	88.8	7.06		213	103	82.2		296	107
Tb (ppb)	0.12	0.18	127	100	323	97.8	19.2		17.0	208	94.7	1		203	101	15.6		234	109
Dy (ppb)	0.37	0.47	732	800	944	106	49.6		43.0	244	97.0	5.15		212	104	90.8		300	104
Ho (ppb)	0.16	0.25	162	200	356	97	7.82		6.0	200	96.2	1.34		200	99.5	21.2		240	110
Er (ppb)	0.34	0.43	440	400	638	99.2	33.5		34.0	225	95.6	4.01		203	99.3	54.8		273	109
Tm (ppb)	0.15	0.26	71.8	80	268	97.9	3.07		2.0	192	94.7	0.69		195	97.4	7.48		232	112
Yb (ppb)	0.31	0.45	422	500	625	102	22.9		18.0	214	95.4	3.8		198	97	44.3		262	109
Lu (ppb)	0.15	0.27	72.1	80	272	100	3.89		3.0	191	93.8	0.62		191	95.1	9.12		230	110

[a]DLOM is the detection limit of the method; DVNM is the determination value with the normal method, which does not add the 200 ng REEs from the stand solutions. DVNM is used for a comparison with the average LREE values in GBW07267 to verify the accuracy. In total, three analysis values were used to calculate the average value. The 200 ng value represents the abundance of each rare earth element in one aliquot of standard solution that was added into the samples. The reference values of GBW07267, GBW07268, and GBW07270 are from http://www.bzwz.com. The reference values of WMS-1a are from http://www.nrcan.gc.ca/home.

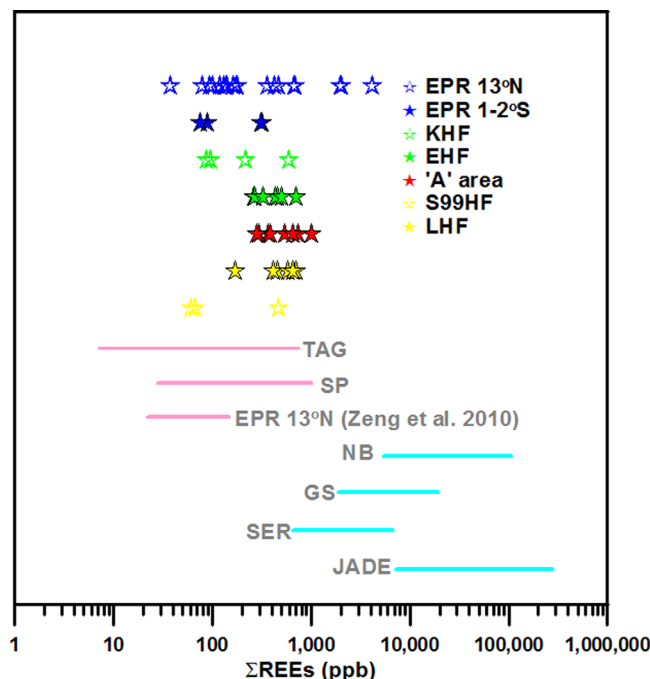**Figure 2.** $\sum$REEs of the sulfides from the EPR 13°N and 1°S–2°S, KHF, EHF, "A" area, S99HF, and LHF. Sources: sulfide data for TAG, Snake Pit (SP), EPR 13°N, and New Brunswick (NB) from *Mills and Elderfield* [1995], *Gillis et al.* [1990], *Zeng et al.* [2010], and *Graf* [1977]. Green Seamount (GS) Si-rich sulfide, Southern Explorer Ridge (SER) sulfides-sulfates, and JADE sulfides-sulfates data from *Alt* [1988], *Barrett et al.* [1990], and *Zeng et al.* [2009]. The symbols indicate the $\sum$REE values in the sulfides from the EPR 13°N and 1°S–2°S, KHF, EHF, "A" area, S99HF, and LHF. The lines indicate the $\sum$REE ranges in the sulfides from TAG, Snake Pit, EPR 13°N and New Brunswick, Green Seamount, Southern Explorer Ridge, and JADE.

REE recovery rates were 79% for Ce and between 91 and 113% for other elements. Using WMS-1a, the REE recovery rates were between 82% and 116% for La-Gd and between 98% and 106% for Tb-Lu. An internal standard (Re solution—5 μg/L) was used throughout the analysis process to monitor instrument stability and signal drift. The RSD was <10%.

The normalized REE data refer to C1-chondrites (subscript CN) [*Sun and McDonough*, 1989]. The Eu and Ce anomalies are defined as (Eu/Eu*)$_{CN}$ = Eu$_{CN}$/(Sm$_{CN}$ + Gd$_{CN}$)$^{0.5}$ and (Ce/Ce*)$_{CN}$ = Ce$_{CN}$/(La$_{CN}$ + Pr$_{CN}$)$^{0.5}$. LREEs include La, Ce, Pr, Nd, Sm, and Eu; HREEs include Gd, Tb, Dy, Ho, Er, Tm, Yb, and Lu. The REE data for the MORB from the EPR, CIR, SWIR, and NFB and for the ultramafic rocks from the MAR were obtained from the updated PetDB database (www.petdb.org).

4. Results

4.1. REE Concentrations in Massive Sulfides

The total REE concentrations ($\sum$REEs) of the seafloor massive sulfide samples in the EPR near 13°N and 1°S–2°S, LHF, KHF, EHF, "A" area, and S99HF are highly variable (37.2–4092 ppb) but are similar to $\sum$REEs of the hydrothermal products (including sulfides, sulfates, and oxides) from the EPR and the MAR (Figure 2). Among our samples, the massive sulfide samples from the EPR near 13°N exhibit both the highest $\sum$REEs (4092 ppb, EPR05-TVG1-3-4) and lowest $\sum$REEs (37.2 ppb, EPR05-TVG2-1-7) (Table 5). The $\sum$REEs (<5 ppm; Table 5) of all the sulfides are far lower those of the basalts [e.g., *Sun et al.*, 2003] and ultramafic rocks [e.g., *Augustin et al.*, 2008] (Figures 3 and 4).

4.2. LREE Enrichment, Eu and Ce Anomalies in the Massive Sulfides

The C1-chondrite-normalized REE distribution patterns of the seafloor massive sulfide samples from the EPR near 13°N and 1°S–2°S, LHF, KHF, EHF, "A" area, and S99HF are shown in Figures 3 and 4. The REE patterns of all the sulfides show evidence of LREE enrichment (LREE/HREE ratios of 2.55–20), variable La$_{CN}$/Lu$_{CN}$ ratios that range between 2.00 and 73.8, Eu anomalies ((Eu/Eu*)$_{CN}$ ratios of 0.34–7.60), and minor or negligible Ce anomalies ((Ce/Ce*)$_{CN}$ ratios of 0.79–1.21).

The sulfides are divided into three types based on these Eu anomalies: Type I has a positive Eu anomaly ((Eu/Eu*)$_{CN}$ > 1.20; Figures 3 and 4), Type II has a weak or negligible Eu anomaly ((Eu/Eu*)$_{CN}$ ≈ 1.00; Figures 3 and 4), and Type III has a negative Eu anomaly ((Eu/Eu*)$_{CN}$ < 0.80; Figure 4). Most of the massive sulfides from the EPR near 13°N are Type I and are characterized by positive Eu anomalies that range between 1.21 and 4.08 (Figures 3 and 4). All the sulfides from the KHF and the LHF, sample IR05-TVG12-3 from the EHF, and sample 113.1GTV-4 from the S99HF are also Type I sulfides. The sulfides from the EPR near 13°N (EPR05-TVG2-1-52) and the EHF (IR05-TVG12-8-4, IR05-TVG12-14, IR05-TVG13-4-2, IR05-TVG13-9.2-1, and IR05-TVG13-9.2-2) are Type II and are characterized by weak or negligible Eu anomalies between 0.81 and 1.18 (Figures 3 and 4). All the sulfides from the EPR near 1°S–2°S, the "A" area of the SWIR near 38°S, and most of the sulfides from S99HF are Type III, with negative Eu anomalies between 0.34 and 0.77 (Figure 4).

Table 5. Chemical Compositions of the Hydrothermal Sulfides From the EPR Near 13°N and 1°S–2°S, KHF, EHF, LHF, "A" Area, and S99HF

	Fe	Cu	Zn	Mn	Al	Ti	Ba	La	Ce	Pr	Nd	Sm	Eu	Gd	Tb	Dy	Ho	Er	Tm	Yb	Lu	ΣREEs	(Eu/Eu*)$_{CN}$	(Ce/Ce*)$_{CN}$
EPR05-TVG, EPR near 13°N, fast spreading ridge (>8 cm/yr)																								
1-2-1[a]	45.9	8,169	4,170	11.6	1,258	29.4	2.11	77.9	166	21.8	80	19.1	7.14	15.7	2.66	13.9	2.9	8.64	1.34	8.68	1.5	427	1.26	0.99
1-2-4	46.7	8,611	15,560	72.3	256	24.9	0.94	26.3	61.1	9.17	35.3	11.4	4.17	7.29	0.78	3.16	0.55	1.58	0.21	1.63	0.21	163	1.4	0.96
1-2-4[b]								28.3	64.6	9.48	39.9	11.7	4.9	8.16	0.68	2.83	0.55	1.77	0.21	1.45	0.27	175	1.53	0.97
1-2-5[a]	45.9	11,430	488	10.1	303	24.5	0.68	20	43.4	6.35	25.9	7.3	3.6	5.26	0.45	2.2	0.49	1.22	0.22	1.29	0.17	118	1.77	0.95
1-3-1[a]	46.2	8,272	6,083	121	341	83.2	1.87	67	163	31.1	161	68	30.4	58.4	6.33	28.4	5.9	17.8	2.91	21.1	3.46	664	1.48	0.87
1-3-3	46.5	16,346	105	8.5	189	36.4	2.47	108	269	36.6	165	36.6	11.1	21.5	1.86	8.83	1.9	6.4	1	5.85	0.97	675	1.21	1.05
1-3-4	46.1	6,299	500	125	1,765	522	1.44	512	1,054	211	951	330	199	287	32.1	171	39.1	123	20.5	140	23.6	4,092	1.97	0.79
1-3-5	46.8	6,134	450	155	898	135	0.76	284	702	101	471	133	68.9	99.2	8.84	39.8	7.42	23.7	3.39	24	3.55	1,970	1.83	1.01
1-3-5[b]								287	712	103	500	140	73.4	100	9.09	41.1	7.81	24.1	3.58	23.7	3.77	2,028	1.9	1.02
1-3-6	46.4	7,759	3,932	180	148	42.1	0.83	42.3	109	15.8	76.6	28.9	14.9	26.5	3.01	15.9	3.25	10.1	1.5	10.4	1.62	360	1.65	1.04
2-1-1[a]	47.1	227	2,801	43.3	96.9	22.1	19.3	23.2	46.6	6.34	26	6.74	5.9	6.7	1.04	6.41	1.24	3.89	0.56	3.96	0.59	139	2.68	0.94
2-1-1[b]								23.8	45.6	6.21	26.6	5.69	5.1	6.37	0.88	5.99	1.19	3.81	0.57	4.1	0.66	137	2.59	0.92
2-1-2	46.2	450	5,977	117	51.1	22.8	9.44	25.4	55.8	7.23	30.5	8	9.47	6.84	1.12	6.7	1.24	3.71	0.54	3.96	0.51	161	3.91	1.01
2-1-3	46.6	613	1,609	184	65.3	23	8.23	23	43.7	5.57	23.5	6.04	3.68	6.36	1.08	6.35	1.19	3.95	0.59	3.98	0.68	130	1.81	0.96
2-1-4	45.9	413	1,425	65.2	165	26.9	16.4	77.2	166	21.37	87.9	21.1	16.2	21.4	3.08	19.1	3.92	11.9	1.84	12.9	2.04	466	2.33	1
2-1-51	46.8	427	5,688	71	176	23.8	14	18.2	37.3	4.19	16.8	3.61	3.37	4.02	0.69	4.18	0.92	2.83	0.44	2.67	0.45	100	2.71	1.05
2-1-52								15.2	33	3.74	15.7	4.24	1.32	4.64	0.66	4.77	1.04	3.51	0.54	3.83	0.55	92.8	0.91	1.07
2-1-6[a]	45.2	1,610	34,790	119	36.2	21.8	4.65	28.7	65.5	8.36	34.4	8.8	9.16	7.9	1.08	6.6	1.17	3.3	0.53	3.92	0.58	180	3.36	1.04
2-1-7	46.2	729	3,657	179	6.55	21.8	0.78	7.08	12.4	1.51	5.66	1.9	0.9	1.84	0.23	1.82	0.44	1.44	0.21	1.55	0.22	37.2	1.47	0.93
2-1-8	45.7	343	6,208	57.2	10	21.8	4.17	12.2	26.2	3.53	15	4.29	5.15	3.47	0.61	3.55	0.72	1.88	0.3	1.99	0.32	79.2	4.08	0.98
20III-S4-TVG, EPR near 1°S–2°S, ultrafast spreading ridge (>8 cm/yr)																								
1-1-2	46.4	8,365	609	139	247	18.8	0.21	19.6	37.2	4.08	15.4	2.82	0.56	2.86	0.33	2.04	0.31	1.22	0.17	1.28	0.2	88	0.6	1.02
1-1-3	46.4	5,130	327	101	296	21.4	0.35	69.6	148	15.2	50.6	8.47	1.73	8.88	0.98	5.09	0.98	2.95	0.38	2.39	0.36	315	0.61	1.12
1-1-3[b]								69.9	142	14.7	50	8.33	1.97	8.5	0.91	5.44	0.97	3.02	0.38	2.38	0.33	308	0.72	1.08
1-1-4	46.6	1,051	531	159	165	17.3	-[c]	17	36.5	3.22	10.6	1.91	0.48	2.09	0.24	1.38	0.27	0.74	0.1	0.65	0.09	75.3	0.74	1.21
IR05-TVG, KHF, intermediate spreading ridge (4–8 cm/yr)																								
9-1	42.3	76,665	3,054	10.8	493	18.2	0.18	10.7	25.2	3.47	17.6	6.56	10.1	5.88	0.56	2.65	0.46	1.17	0.27	1.17	0.2	86	4.95	1.01
9-1[b]								11.4	28.1	4.04	19.7	7.43	12	6.12	0.79	2.97	0.45	1.06	0.22	0.96	0.17	95.4	5.46	1.02
9-2	42.5	99,827	2,887	7.98	388	16.9	0.09	32.6	78.3	11.1	54.2	13.2	12.8	8.81	0.58	2.05	0.32	1.03	0.23	0.9	0.14	216	3.65	1.01
9-3[a]	42.7	70,004	30,130	10.7	331	17.7	0.38	97.5	234	32.2	147	34.1	15.4	19	1.24	3.54	0.51	1.89	0.27	1.33	0.14	588	1.86	1.02
IR05-TVG, EHF, intermediate spreading ridge (4–8 cm/yr)																								
12-3	3.47	600	29,501	7.12	121	2	2,124	71.4	114	17.7	89.7	35.8	58.5	31.8	2.81	14.1	2.29	5.93	0.79	5.26	0.8	451	5.3	0.79
12-3[b]								77.4	123	17.6	86.5	31.6	37.6	29.5	2.36	12.3	2.1	5.51	0.75	4.88	0.78	432	3.77	0.82
12-8-4	17.5	899	413,300	23	96.3	7.47	532	48.1	110	12.7	48.1	14.9	2.84	7.6	0.97	6	1.29	3.81	0.54	4.12	0.69	262	0.81	1.09
12-14[a]	11.9	938	432,404	38.2	58.1	4.34	1.6	64.9	117	11.5	40.1	9.48	2.68	6.89	0.92	5.16	0.99	3.57	0.46	3.53	0.59	268	1.01	1.05
13-4-2	33.9	121,922	31,679	29.8	269	14.1	323	153	348	33	103	16.4	4.25	15.5	1.67	9.38	1.81	6.01	0.85	6.12	1.03	699	0.82	1.2
13-9.2-1[a]	36.4	39,067	10,404	54.1	44.6	17.3	259	105	232	22.6	76.84	14.3	3.82	14.5	1.69	9.91	1.83	5.88	1.01	6.78	1.13	498	0.81	1.17
13-9.2-2	36.5	30,140	28,901	109	30.7	16.8	328	73.4	145	15.1	54.1	9.67	3.62	9.12	1.09	5.78	1.13	3.22	0.45	3.3	0.5	326	1.18	1.07
20V-S35-TVG, "A" area, ultraslow spreading ridge (1–4 cm/yr)																								
17-1-1	42.1	15,910	-	10.6	1,110	12.7	-	236	435	45.1	155	28.6	4.97	28.4	3.31	20.96	4.46	14.1	2.2	16.4	2.65	997	0.53	1.03
17-1-2	40.4	2,447	1,014	18.3	27.2	17	0.67	80.1	165	15.8	58.7	11.2	2.41	11	1.3	7.78	1.59	5.24	0.72	5.06	0.8	366	0.66	1.13
17-1-2[b]								86.4	176	16.5	56.7	11.7	2.84	10.8	1.33	7.34	1.25	4.32	0.61	4.25	0.68	380	0.77	1.14
17-2	44.5	20,162	277	10.9	119	10.4	0.05	170	328	31.3	109	19.6	3.31	23.4	2.48	15.2	3.02	9.9	1.57	11.7	1.97	731	0.47	1.1
17-3-2[a]	41.3	2,637	2,480	16.8	202	15	0.31	125	238	24.4	84.7	15.1	3.07	14.8	1.84	9.88	2.01	6.02	1.01	7.35	1.17	534	0.63	1.06
17-4-2[a]	41.1	2,580	1,386	11.4	29	18.4	-	65.2	131	13.6	46.5	8.24	1.5	8.46	1.01	6.45	1.27	3.92	0.6	4.75	0.74	293	0.55	1.08
17-5-1	-	-	-	10.4	1,110	6.99	-	64	127	12.4	41.5	7.96	1.6	8.2	0.96	5.33	1.12	3.26	0.47	3.79	0.64	278	0.61	1.11
17-5-2	43.2	27,687	21,655	13.5	1,146	9.65	1.52	149	303	28.5	96.9	17.2	2.99	16.6	2.43	12.9	2.3	7.82	1.08	8.91	1.31	651	0.54	1.14
17-6	45.2	15,098	244	10.4	97.6	8.6	0.06	62.5	127	12.2	41.3	7.55	0.99	9.09	0.95	5.88	1.28	3.83	0.58	4.34	0.73	278	0.37	1.13
MAR05-TVG, LHF, slow spreading ridge (1–4 cm/yr)																								
1-9[a]	31	314,180	1,422	88.8	7.88	30.2	3.25	8.57	16.2	2.41	10.8	2.97	2.05	3.33	0.64	4.72	1.04	3.18	0.45	3.06	0.46	59.8	2	0.87
1-9[b]								9.77	18.8	2.77	12.7	3.18	2.04	3.58	0.72	4.65	0.96	3.16	0.45	3.2	0.4	66.4	1.85	0.89
1-10-2[a]	37.3	125,219	267	374	1,512	120	11.4	60.5	132	17	78.1	19.4	52.8	23.3	4.16	27.5	5.79	17.1	2.63	18.1	2.9	462	7.6	1.01
S99HF, NFB, back-arc basin																								
26.2GTV-2	6.28	8,530	535,700	102	163	5.79	3.42	38.3	79.5	6.8	24.7	4.93	0.86	4.13	0.46	3.22	0.61	2.25	0.29	2.03	0.42	169	0.58	1.21
42GTV-1	39	48,071	5,146	13.4	159	16.8	90.5	109	207	20	69.9	12.3	2.72	12.2	1.33	8.13	1.74	5.48	0.84	6.1	1.03	457	0.68	1.09
42GTV-1[b]								111	205	20.3	70.1	12.1	2.9	12.8	1.38	7.86	1.57	4.95	0.76	5.96	1.05	458	0.71	1.06
42GTV-2	37.1	114,736	4,558	14	5.28	15.9	142	95.8	187	18.5	64.8	12.6	1.89	11.8	1.18	7.61	1.61	5.17	0.75	5.57	0.91	415	0.47	1.09
42GTV-3[a]	29.3	197,581	10,239	7.1	113	11.6	2.29	96	185	18	62.7	11.4	1.3	11.9	1.24	8.27	1.67	5.17	0.84	5.91	1.01	411	0.34	1.09
113.1GTV-1[a]	37.9	10,357	7,875	111	399	16.7	11.9	149	291	29.3	101	18.9	2.87	19.1	2.27	13.5	2.71	8.21	1.25	9.74	1.61	650	0.46	1.08
113.1GTV-2[a]	36	22,903	3,734	87.6	275	17.2	8.61	136	259	26.1	88.9	16.7	2.9	16.3	1.7	10.9	2.14	7.17	1.13	8.24	1.3	578	0.54	1.07
113.1GTV-4	5.24	13,725	16,830	232	3,224	9.51	6.16	69.4	207	32	152	44.5	56.4	46.1	7.03	38.9	7.01	19.3	2.93	21.6	3.62	708	3.81	1.08
113.2GTV[a]	38.3	20,238	15,960	244	228	16.7	3.11	152	296	29.5	101	20.5	3.78	19.5	2.03	12.6	2.66	8.4	1.19	9.33	1.72	659	0.58	1.08

[a]Indicates the Fe, Cu, Zn data from *Zeng et al.* [2014].
[b]Indicates the analysis result of a parallel sample.
[c]"-" indicates no data available. The units are % for Fe; ppm for Cu, Zn, Mn, Al, Ti, and Ba; and ppb for La, Ce, Pr, Nd, Sm, Eu, Gd, Tb, Dy, Ho, Er, Tm, Yb, Lu, and ΣREEs.
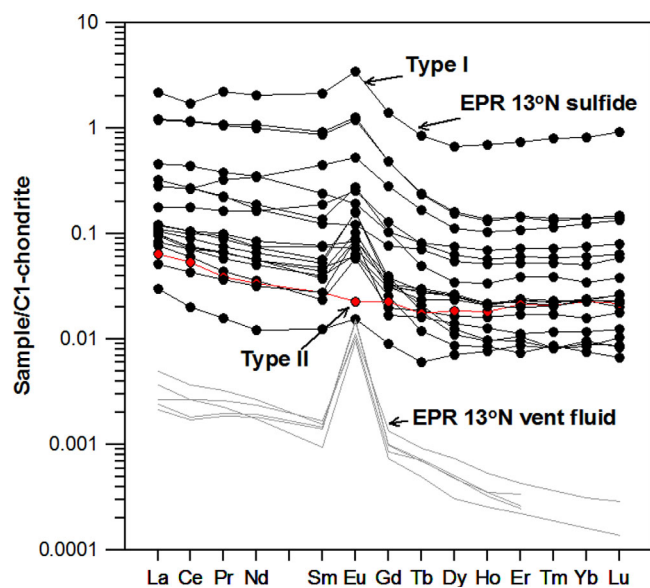
Figure 3. REE patterns in Type I and Type II (red lines) sulfides from the EPR near 13°N. Sources: vent fluid data from *Douville et al.* [1999], *Klinkhammer et al.* [1994], and *Michard and Albarède* [1986]. Normalization data from *Sun and McDonough* [1989].

5. Discussion

5.1. Variable REE Concentrations and Fractionation Between LREEs and HREEs in Seafloor Sulfides

The $\sum$REEs in our sulfide samples vary considerably (37.2–4092 ppb), and the $\sum$REEs exhibit no systematic variation with Fe, Cu, and Zn. The $\sum$REEs and associated ranges in Fe-rich sulfides (e.g., pyrite) (Table 5) all exceed the $\sum$REEs and associated ranges in Cu (i.e., chalcopyrite) and Zn-rich (i.e., sphalerite) sulfides, which precipitated from high-temperature (>300°C) and medium-temperature (300–200°C) fluids, respectively [e.g., *Fouquet et al.*, 1988; *Kim et al.*, 2006]. Therefore, the high $\sum$REEs and ranges in the seafloor massive sulfides are likely related to Fe-rich sulfide minerals, which is consistent with the fact that Fe-rich sulfide minerals show a wide range of formation temperatures (<100°C to >300°C) [e.g., *Fouquet et al.*, 1988; *Hannington et al.*, 1991].

Furthermore, the substitution of REEs into Fe, Cu, and Zn-rich sulfides appears to be strongly influenced by the larger ionic radii of the REEs [e.g., *Alt*, 1988; *Mills and Elderfield*, 1995]. The degrees of fractionation between the LREEs and HREEs in the seafloor massive sulfides from the EPR near 13°N and 1°S–2°S, LHF, KHF, EHF, "A" area, and S99HF are highly variable (Figures 3 and 4). The greatest fractionation difference between the LREEs and HREEs (LREE/HREE = 20, sample IR05-TVG9-3; Table 5) is present in the KHF sulfides, which consist of abundant pyrite, and the smallest fractionation difference (LREE/HREE = 2.55, sample MAR05-TVG1-9; Table 5) is present in the LHF sulfides, which consist of abundant chalcopyrite. Thus, greater HREE enrichment occurs in Cu-rich sulfide minerals than in Fe-rich sulfide minerals, which is consistent with the fact that the ionic radius of Cu^{2+} (73 pm) and Zn^{2+} (74 pm) are similar to that of Lu^{3+} (86.1 pm), whereas the ionic radius of Fe^{2+} is much smaller (55 pm) [*Rimskaya-Korsakova and Dubinin*, 2003].

5.2. Origin of Eu Anomalies

The REE patterns in most sulfides from the EPR near 13°N (e.g., EPR05-TVG2-1-1 and EPR05-TVG2-1-2) and all the sulfides from the LHF exhibit positive Eu anomalies of 1.26–7.60 (Figures 3 and 4), similar to the sulfide-forming fluids at the EPR near 13°N and the LHF [*Michard and Albarède*, 1986; *Klinkhammer et al.*, 1994; *Douville et al.*, 1999; *Schmidt et al.*, 2007]. These similarities suggest that these sulfides inherited their positive Eu anomalies from the sulfide-forming fluids [e.g., *Barrett et al.*, 1990; *Gillis et al.*, 1990; *Mills and Elderfield*, 1995]. Furthermore, the stability of soluble Eu^{2+} species has been found to increase in association with Cl^- complexing, low to high-temperature acidic fluids, and reducing conditions [e.g., *Sverjensky*, 1984; *Schade et al.*, 1989; *Wood and Williams-Jones*, 1994; *Haas et al.*, 1995; *Mills and Elderfield*, 1995; *Allen and Seyfried*, 2005]. Therefore, the positive Eu anomalies in the sulfides were likely formed by Cl^- complexing under high-temperature, low-pH, and strongly reducing conditions [e.g., *Mills and Elderfield*, 1995].

The sulfides from the EPR near 13°N (EPR05-TVG1-3-3 and EPR05-TVG2-1-52) and the EHF (IR05-TVG12-8-4, IR05-TVG12-14, IR05-TVG13-4-2, IR05-TVG13-9.2-1, and IR05-TVG13-9.2-2) are characterized by weak or negligible Eu anomalies of 0.81–1.21 (Figures 3 and 4). All the sulfides from the EPR near 1°S–2°S, the "A" area of the SWIR near 38°S, and most of the sulfides from S99HF in the NFB exhibit negative Eu anomalies of 0.34–0.77 (Figure 4) and positive Gd anomalies (Figure 4), which are both considered to be signals of low-temperature seawater [*de Baar et al.*, 1985]. Furthermore, a large proportion of the Eu in the low-temperature fluid is trivalent because divalent Eu is stable at temperatures above approximately 250°C

Figure 4. REE patterns in (a) Type III sulfides from the EPR near 1°S–2°S, (b) Type I sulfides from the KHF, (c) Type I and Type II sulfides from the EHF, (d) Type III sulfides from the "A" area, (e) Type I sulfides from the LHF, and (f) Type I and Type III sulfides from the S99HF. Sources: vent fluid data from *Schmidt et al.* [2007]. Normalization data from *Sun and McDonough* [1989].

[*Sverjensky*, 1984]. Decreases in the formation temperatures of the hydrothermal sulfides, i.e., from medium (200–300°C) to low temperatures (<280°C in the EPR near 13°N and <12°C in the NFB; Table 2), directly correlate with decreases in the Eu^{2+}/Eu^{3+} ratios in the sulfide-forming fluids [e.g., *Mills and Elderfield*, 1995]. Thus, the accumulation of Eu^{2+} in sulfides that formed at medium to low temperatures is also reduced, which is consistent with the fact that negligible or negative Eu anomalies are related to lower Eu contents in the sulfides (Figure 5).
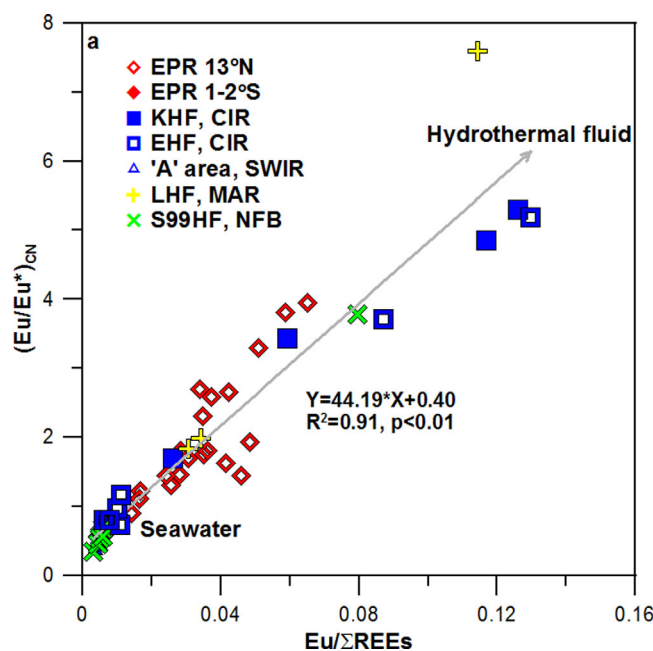
Figure 5. Eu anomalies in seafloor massive sulfides versus Eu/∑REEs ratios. The solid gray line indicates a correlation between elevated Eu anomalies and elevated Eu concentrations in the sulfides.

Consequently, the Eu concentrations of the sulfide-forming fluids may influence the Eu anomalies in the resulting sulfides. The negligible or negative Eu anomalies in the sulfides can be interpreted as the results of medium to low-temperatures and less Eu enriched fluids [*Michard and Albarède*, 1986; *Gillis et al.*, 1990] due to mixing between hydrothermal fluids and seawater. Furthermore, seafloor hydrothermal recrystallization (i.e., zone refining) may also have caused remobilization of REEs, particularly Eu^{2+}, producing negligible or negative Eu anomalies in the sulfides [*Mills and Elderfield*, 1995].

5.3. Sources of REEs in Sulfides

The REEs in the sulfides may reflect the sources and evolution of hydrothermal fluids [e.g., *Mills and Elderfield*, 1995]. Previous studies on REEs in sulfides from the Rainbow, Broken Spur, and TAG hydrothermal fields on the MAR have suggested that the REEs are all derived from hydrothermal fluids [*Barrett et al.*, 1990; *Rimskaya-Korsakova and Dubinin*, 2003] and are incorporated into sulfide mineral crystals during the mixing of the hydrothermal fluids and seawater. Comparisons show that the REE patterns of the massive sulfides from the EPR near 13°N and 1°S–2°S, the LHF, the KHF, the EHF, the "A" area, and the S99HF are similar to those of vent fluids (Figures 3 and 4). Thus, the REEs in the seafloor massive sulfides are likely all derived from hydrothermal fluids that leached REEs from subseafloor wall rocks (MORBs or ultramafic rocks) and deposited them in the sulfides [*Piepgras and Wasserburg*, 1985; *Langmuir et al.*, 1997].

5.4. REE Flux

The analysis of our 46 massive sulfide samples from modern seafloor hydrothermal fields permits realistic estimation of the magnitude of hydrothermal REE flux into the ocean water. The simple calculation below presumes that vent fluids readily supply REEs to massive sulfide deposits. Data from the new massive sulfide deposits from 10,000 km of ridge, arc, and back-arc spreading centers indicate that the amount of massive sulfide deposits on the seafloor of the world's oceans is on the order of 6×10^8 t [*Hannington et al.*, 2011]. The formula for estimating the approximate amount of REEs in seafloor massive sulfide is

$$S_{REEs} = M_{sulfide} \times X_{REEs} \tag{1}$$

where S_{REEs} is the mass of REEs that hydrothermal fluids have supplied to the massive sulfide deposits, $M_{sulfide}$ is the total mass of seafloor massive sulfide deposits (6×10^8 t) [*Hannington et al.*, 2011], and X_{REEs} is the ∑REEs of the massive sulfides. Calculations were performed for each sample using the observed REE concentrations (∑REE = 37.1–4092 ppb) in the seafloor massive sulfides from the EPR near 13°N and 1°S–2°S, MAR, CIR, SWIR, and BAB, and an averaged calculation was conducted for all 46 massive sulfide samples. These calculations estimate that approximately 20–2500 t (an average of 280 t, $n = 46$) of REEs from hydrothermal fluids have been supplied to the sulfide deposits. Moreover, the slow (1–4 cm/yr), intermediate (4–8 cm/yr), and fast (>8 cm/yr) spreading ridges account for 86%, 12%, and <2%, respectively, of the total tonnage (6×10^8 t) of seafloor massive sulfides [*Hannington et al.*, 2011]. The ∑REEs of the massive sulfides from the slow (e.g., the "A" area and LHF), intermediate (e.g., the KHF and EHF), and fast (e.g., the EPR near 13°N and 1°S–2°S) spreading ridges are approximately 66–997 ppb (avg 425 ppb, $n = 12$), 86–699 ppb (avg 356 ppb, $n = 11$), and 37–4092 ppb (avg 541 ppb, $n = 24$), respectively (see Table 5). According to formula (1), we estimate that an average of 219 t ($n = 12$), 26 t ($n = 11$), and 6.49 t ($n = 24$) of REEs have been

supplied by hydrothermal fluids to the sulfide deposits in the slow, intermediate, and fast spreading ridges, respectively.

The flux of hydrothermal fluid at the mid-ocean ridges is currently on the order of $6-12 \times 10^{10}$ t yr^{-1} [*Elderfield and Schultz*, 1996]. Assuming an average REE concentration of 3 ng/g in the hydrothermal fluids (0.27–33 ng/g, $n = 84$) [*Michard and Albarède*, 1986; *Michard*, 1989; *Klinkhammer et al.*, 1994; *Mitra et al.*, 1994; *James et al.*, 1995; *Bau and Dulski*, 1999; *Douville et al.*, 1999, 2002; *Schmidt et al.*, 2007], the global REE flux from hydrothermal vents into the oceans is approximately 180–360 t yr^{-1}. These figures suggest that the hydrothermal vents at MORs alone transport larger quantities of REEs to the oceans over the course of just 2 years than is estimated to be present in all the seafloor hydrothermal sulfide deposits at ocean ridges. The fate of the excess REEs (i.e., REEs not captured by massive sulfides) is unclear, but sulfate deposits and metalliferous sediment are known to be enriched in REEs deposited from hydrothermal fluids and plumes that are associated with MOR and BAB hydrothermal systems [e.g., *Ruhlin and Owen*, 1986; *Owen and Olivarez*, 1988; *Barrett et al.*, 1990; *Mills and Elderfield*, 1995; *Bach et al.*, 2003; *Kato et al.*, 2011]. These sulfate deposits and metalliferous sediment may account for a large fraction of the REEs that are not represented in the massive sulfide deposits [e.g., *Barrett et al.*, 1987; *German et al.*, 1990; *Bach et al.*, 2003].

6. Conclusions

A total of 46 seafloor massive sulfides show a widely varying range of $\sum$REEs (37.2–4092 ppb). These deposits are notably more enriched in LREEs than HREEs and exhibit positive, weak/negligible, or negative Eu anomalies and weak or negligible Ce anomalies. The variation in the proportions of LREEs and HREEs is consistent with those observed in hydrothermal fluids, indicating that the REEs in global seafloor massive sulfides are sourced from hydrothermal fluids and that the LREE/HREE ratios are inherited by the precipitated massive sulfides from the hydrothermal fluids. The REE concentrations and patterns of seafloor massive sulfides are related to the mineral chemistry but are also influenced by the physicochemical composition, REE concentrations and REE patterns of the sulfide-forming fluids, the degree of mixing between the hydrothermal fluids and seawater, and interactions with subseafloor rocks. Of these factors, we propose that the mineral chemistry and the REE concentrations and patterns of the sulfide-forming fluids are the principal factors that control the REE chemistry of massive sulfides.

A positive correlation between Eu anomalies and Eu concentrations is observed ($R^2 = 0.91$, $p < 0.01$). Three types of REE patterns related to variations in the Eu anomalies are recognized in the sulfides. Type I exhibits positive Eu anomalies (($Eu/Eu^*)_{CN} > 1.20$). These positive Eu anomalies occur in sulfides precipitated at high temperatures in association with acidic or reducing fluids. Type II exhibits weak or negligible anomalies (($Eu/Eu^*)_{CN} \approx 1.00$), and Type III exhibits negative Eu anomalies (($Eu/Eu^*)_{CN} < 0.80$). Weak, negligible (Type II), or negative Eu (Type III) anomalies in sulfides are indicative of lower Eu concentrations, medium to low-temperature conditions, mixing between the hydrothermal fluids and seawater and the mineral chemistry. Therefore, Eu anomaly values could possibly be used to infer the REE properties of the sulfide-forming fluids, for example, positive Eu anomalies in all the sulfides from the KHF formed from high-temperature (>300°C) acidic (pH < 3.6) fluids (see Table 2).

Based on analyses of the REE concentrations in the seafloor massive sulfides, we estimate that all the seafloor massive sulfide deposits in the world contain approximately 280 t of REEs. Therefore, discovering a deposit that contains large amounts (>20 t) of rare earth elements in seafloor hydrothermal fields is unlikely. The global flux of REEs from hydrothermal vents is up to 180–360 t yr^{-1}. Over the course of 2 years, the minimum amount (>360 t) of REEs from hydrothermal vents is far greater than the sum total contained in all the sulfide deposits. The excess quantities of REEs (i.e., REEs not captured by massive sulfides) might be partially hosted by sulfate deposits and metalliferous sediments far from the hydrothermal vents, implying that global seafloor massive sulfides are not a significant sink of hydrothermal REEs.

References

Allen, D. E., and W. E. Seyfried Jr. (2005), REE controls in ultramafic hosted MOR hydrothermal systems: An experimental study at elevated temperature and pressure, *Geochim. Cosmochim. Acta*, *69*(3), 675–683, doi:10.1016/j.gca.2004.07.016.
Alt, J. C. (1988), The chemistry and sulfur isotope composition of massive sulfide and associated deposits on Green seamount, eastern Pacific, *Econ. Geol.*, *83*(5), 1026–1033, doi:10.2113/gsecongeo.83.5.1026.

Augustin, N., K. S. Lackschewitz, T. Kuhn, and C. W. Devey (2008), Mineralogical and chemical mass changes in mafic and ultramafic rocks from the Logatchev hydrothermal field (MAR 15°N), *Mar. Geol.*, *256*(1–4), 18–29, doi:10.1016/j.margeo.2008.09.004.

Bach, W., S. Roberts, D. A. Vanko, R. A. Binns, C. J. Yeats, P. R. Craddock, and S. E. Humphris (2003), Controls of fluid chemistry and complexation on rare-earth element contents of anhydrite from the Pacmanus subseafloor hydrothermal system, Manus basin, Papua New Guinea, *Miner. Deposita*, *38*(8), 916–935, doi:10.1007/s00126-002-0325-0.

Barrett, T. J., P. N. Taylor, and J. Lugoqski (1987), Metalliferous sediments from DSDP leg 92: The East Pacific Rise transect, *Geochim. Cosmochim. Acta*, *51*(9), 2241–2253, doi:10.1016/0016-7037(87)90278-X.

Barrett, T. J., I. Jarvis, and K. E. Jarvis (1990), Rare earth element geochemistry of massive sulfides-sulfates and gossans on the Southern Explorer Ridge, *Geology*, *18*(7), 583–586, doi:10.1130/0091-7613(1990)018<0583:REEGOM>2.3.CO;2.

Bau, M., and P. Dulski (1999), Comparing yttrium and rare earths in hydrothermal fluids from the Mid-Atlantic Ridge: Implications for Y and REE behaviour during near-vent mixing and for the Y/Ho ratio of Proterozoic seawater, *Chem. Geol.*, *155*(1–2), 77–90, doi:10.1016/S0009-2541(98)00142-9.

Bowers, T. S., A. C. Campbell, C. I. Measures, A. J. Spivack, M. Khadem, and J. M. Edmond (1988), Chemical controls on the composition of vent fluids at 13°–11°N and 21°N, East Pacific Rise, *J. Geophys. Res.*, *93*(B5), 4522–4536, doi:10.1029/JB093iB05p04522.

Charlou, J. L., J. P. Donval, Y. Fouquet, P. Jean-Baptiste, and N. Holm (2002), Geochemistry of high H_2 and CH_4 vent fluids issuing from ultramafic rocks at the Rainbow hydrothermal field (36°14′N, MAR), *Chem. Geol.*, *191*(4), 345–359, doi:10.1016/S0009-2541(02)00134-1.

Cole, C. S., R. H. James, D. P. Connelly, and E. C. Hathorne (2014), Rare earth elements as indications of hydrothermal processes within the east Scotia subduction zone systems, *Geochim. Cosmochim. Acta*, *140*, 20–38.

Craddock, P. R., W. Bach, J. S. Seewald, O. J. Rouxel, E. Reeves, and M. K. Tivey (2010), Rare earth element abundances in hydrothermal fluids from the Manus basin, Papua New Guinea: Indicators of sub-seafloor hydrothermal processes in back-arc basins, *Geochim. Cosmochim. Acta*, *74*(19), 5494–5513, doi:10.1016/j.gca.2010.07.003.

de Baar, H. J. W., P. G. Brewer, and M. P. Bacon (1985), Anomalies in rare earth distributions in seawater: Gd and Tb, *Geochim. Cosmochim. Acta*, *49*(9), 1961–1969, doi:10.1016/0016-7037(85)90090-0.

Douville, E., P. Bienvenu, J. L. Charlou, J. P. Donval, Y. Fouquet, P. Appriou, and T. Gamo (1999), Yttrium and rare earth elements in fluids from various deep-sea hydrothermal systems, *Geochim. Cosmochim. Acta*, *63*(5), 627–643, doi:10.1016/S0016-7037(99)00024-1.

Douville, E., J. L. Charlou, E. H. Oelkers, P. Bienvenu, C. F. Jove Colon, J. P. Donval, Y. Fouquet, D. Prieur, and P. Appriou (2002), The rainbow vent fluids (36°14′N, MAR): The influence of ultramafic rocks and phase separation on trace metal content in Mid-Atlantic Ridge hydrothermal fluids, *Chem. Geol.*, *184*(1–2), 37–48, doi:10.1016/S0009-2541(01)00351-5.

Eissen, J., M. Nohara, J. Cotten, and K. Hirose (1994), North Fiji basin basalts and their magma sources: Part I. Incompatible element constraints, *Mar. Geol.*, *116*(1–2), 153–178, doi:10.1016/0025-3227(94)90174-0.

Elderfield, H., and A. Schultz (1996), Mid-ocean ridge hydrothermal fluxes and the chemical composition of the ocean, *Annu. Rev. Earth Planet. Sci.*, *24*(1), 191–224, doi:10.1146/annurev.earth.24.1.191.

Elderfield, H., M. Whitfield, J. D. Burton, M. P. Bacon, and P. S. Liss (1988), The oceanic chemistry of the rare earth elements, *Philos. Trans. R. Soc. London A*, *325*, 105–126.

Embley, R., et al. (2007), Exploring the Submarine Ring of Fire: Mariana Arc-Western Pacific, *Oceanography*, *20*(4), 68–79, doi:10.5670/oceanog.2007.07.

Fouquet, Y., G. Auclair, P. Cambon, and J. Etoubleau (1988), Geological setting and mineralogical and geochemical investigations on sulfide deposits near 13°N on the East Pacific Rise, *Mar. Geol.*, *84*(3–4), 145–178, doi:10.1016/0025–3227(88)90098-9.

Gallant, R. M., and K. L. Von Damm (2006), Geochemical controls on hydrothermal fluids from the Kairei and Edmond vent fields, 23°-25°S, Central Indian Ridge, *Geochem. Geophys. Geosyst.*, *7*, Q06018, doi:10.1029/2005GC001067.

German, C. R., G. P. Klinkhammer, J. M. Edmond, A. Mura, and H. Elderfield (1990), Hydrothermal scavenging of rare-earth elements in the ocean, *Nature*, *345*(6275), 516–518, doi:10.1038/345516a0.

Gillis, K. M., A. D. Smith, and J. N. Ludden (1990), Trace element and Sr isotopic contents of hydrothermal clays and sulfides from the Snakepit hydrothermal field: ODP site 649, *Proc. Ocean Drill. Program Sci. Results*, *106*(109), 315–319.

Graf, J. L. (1977), Rare earth elements as hydrothermal tracers during the formation of massive sulfide deposits in volcanic rocks, *Econ. Geol.*, *72*(4), 527–548, doi:10.2113/gsecongeo.72.4.527.

Haas, J. R., E. L. Shock, and D. C. Sassani (1995), Rare earth elements in hydrothermal systems: Estimates of standard partial molal thermodynamic properties of aqueous complexes of the rare earth elements at high pressures and temperatures, *Geochim. Cosmochim. Acta*, *59*(21), 4329–4350, doi:10.1016/0016-7037(95)00314-P.

Hannington, M., J. Jamieson, T. Monecke, S. Petersen, and S. Beaulieu (2011), The abundance of seafloor massive sulfide deposits, *Geology*, *39*(12), 1155–1158, doi:10.1130/G32468.1.

Hannington, M. D., P. Herzig, S. Scott, G. Thompson, and P. Rona (1991), Comparative mineralogy and geochemistry of gold-bearing sulfide deposits on the mid-ocean ridges, *Mar. Geol.*, *101*, 217–248.

Henderson, P. (1984), General geochemical properties and abundances of the rare earth elements, in *Rare Earth Element Geochemistry*, edited by P. Henderson, pp. 1–32, Elsevier, Amsterdam.

Hofmann, A. W. (1988), Chemical differentiation of the Earth: The relationship between mantle, continental crust, and oceanic crust, *Earth Planet. Sci. Lett.*, *90*(3), 297–314, doi:10.1016/0012-821X(88)90132-X.

Humphris, S. E. (1998), Rare earth element composition of anhydrite: Implications for deposition and mobility within the active TAG hydrothermal mound, *Proc. Ocean Drill. Program Sci. Results*, *158*, 143–159.

Humphris, S. E., and W. Bach (2005), On the Sr isotope and REE compositions of anhydrites from the TAG seafloor hydrothermal system, *Geochim. Cosmochim. Acta*, *69*(6), 1511–1525, doi:10.1016/j.gca.2004.10.004.

Ishibashi, J., D. Grimaud, Y. Nojiri, J.-M. Auzende, and T. Urabe (1994a), Fluctuation of chemical compositions of the phase-separated hydrothermal fluid from the North Fiji Basin Ridge, *Mar. Geol.*, *116*, 215–226.

Ishibashi, J., H. Wakita, Y. Nojiri, D. Grimaud, P. Jean-Baptiste, T. Gamo, J.-M. Auzende, and T. Urabe (1994b), Helium and carbon geochemistry of hydrothermal fluids from the North Fiji basin spreading ridge (southwest pacific), *Earth Planet. Sci. Lett.*, *128*, 183–197.

James, R. H., H. Elderfield, and M. R. Palmer (1995), The chemistry of hydrothermal fluids from the broken Spur site, 29°N Mid-Atlantic Ridge, *Geochim. Cosmochim. Acta*, *59*(4), 651–659, doi:10.1016/0016-7037(95)00003-I.

Kato, Y., K. Fujinaga, K. Nakamura, Y. Takaya, K. Kitamura, J. Ohta, R. Toda, T. Nakashima, and H. Iwamori (2011), Deep-sea mud in the Pacific Ocean as a potential resource for rare-earth elements, *Nat. Geosci.*, *4*(8), 535–539, doi:10.1038/ngeo1185.

Kim, J., I. Lee, P. Halbach, K. Lee, Y. Ko, and K. Kim (2006), Formation of hydrothermal vents in the North Fiji basin: Sulfur and lead isotope constraints, *Chem. Geol.*, *233*(3–4), 257–275, doi:10.1016/j.chemgeo.2006.03.011.

Klinkhammer, G. P., H. Elderfield, J. M. Edmond, and A. Mitra (1994), Geochemical implications of rare earth element patterns in hydrothermal fluids from mid-ocean ridges, *Geochim. Cosmochim. Acta*, *58*(23), 5105–5113, doi:10.1016/0016-7037(94)90297-6.

Koschinsky, A., R. Seifert, P. Halbach, M. Bau, S. Brasse, L. M. de Carvalho, and N. M. Fonseca (2002), Geochemistry of diffuse low-temperature hydrothermal fluids in the North Fiji basin, *Geochim. Cosmochim. Acta*, *66*(8), 1409–1427, doi:10.1016/S0016-7037(01)00855-9.

Koschinsky, A., D. Garbe-Schönberg, S. Sander, K. Schmidt, H. Gennerich, and H. Strauss (2008), Hydrothermal venting at pressure-temperature conditions above the critical point of seawater, 5°S on the Mid-Atlantic Ridge, *Geology*, *36*(8), 615–618, doi:10.1130/G24726A.1.

Kumagai, H., et al. (2008), Geological background of the Kairei and Edmond hydrothermal fields along the Central Indian Ridge: Implications of their vent fluids' distinct chemistry, *Geofluids*, *8*(4), 239–251, doi:10.1111/j.1468-8123.2008.00223.x.

Langmuir, C., et al. (1997), Hydrothermal vents near a mantle hot spot: The Lucky strike vent field at 37°N on the Mid-Atlantic Ridge, *Earth Planet. Sci. Lett.*, *148*(1–2), 69–91, doi:10.1016/S0012-821X(97)00027-7.

Merlivat, L., F. Pineau, and M. Javoy (1987), Hydrothermal vent waters at 13°N on the East Pacific Rise: Isotopic composition and gas concentration, *Earth Planet. Sci. Lett.*, *84*(1), 100–108, doi:10.1016/0012-821X(87)90180-4.

Michard, A. (1989), Rare earth element systematics in hydrothermal fluids, *Geochim. Cosmochim. Acta*, *53*(3), 745–750, doi:10.1016/0016-7037(89)90017-3.

Michard, A., and F. Albarède (1986), The REE content of some hydrothermal fluids, *Chem. Geol.*, *55*(1–2), 51–60, doi:10.1016/0009–2541(86)90127-0.

Michard, A., F. Albarède, G. Michard, J.-F. Minster and J.-L. Charlou (1983), Rare-earth elements and uranium in high-temperature solutions from East Pacific Rise hydrothermal vent field (13°N), *Nature*, *303*(5920), 795–797, doi:10.1038/303795a0.

Michard, G., F. Albarède, A. Michard, J.-F. Minster, J.-L. Charlou and N. Tan (1984), Chemistry of solutions from the 13°N East Pacific Rise hydrothermal site, *Earth Planet. Sci. Lett.*, *67*(3), 297–307, doi:10.1016/0012-821X(84)90169-9.

Mills, R. A., and H. Elderfield (1995), Rare earth element geochemistry of hydrothermal deposits from the active TAG mound, 26°N Mid-Atlantic Ridge, *Geochim. Cosmochim. Acta*, *59*(17), 3511–3524, doi:10.1016/0016-7037(95)00224-N.

Mitra, A., H. Elderfield, and M. J. Greaves (1994), Rare earth elements in submarine hydrothermal fluids and plumes from the Mid-Atlantic Ridge, *Mar. Chem.*, *46*(3), 217–235, doi:10.1016/0304-4203(94)90079-5.

Mozgova, N. N., and A. V. Efimov (1999), Mineralogy and chemistry of massive sulfides from the Logatchev hydrothermal field (14°45′N Mid-Atlantic Ridge), *Explor. Min. Geol.*, *8*(3-4), 379–395.

Nakamura, K., T. Morishita, W. Bach, F. Klein, K. Hara, K. Okino, K. Takai, and H. Kumagai (2009), Serpentinized troctolites exposed near the Kairei Hydrothermal Field, Central Indian Ridge: Insights into the origin of the Kairei hydrothermal fluid supporting a unique microbial ecosystem, *Earth Planet. Sci. Lett.*, *280*(1–4), 128–136, doi:10.1016/j.epsl.2009.01.024.

Nohara, M., K. Hirose, J.-P. Eissen, T. Urabe, and M. Joshima (1994), The North Fiji Basin basalts and their magma sources: Part II. Sr-Nd isotopic and trace element constraints, *Mar. Geol.*, *116*(1–2), 179–195, doi:10.1016/0025-3227(94)90175-9.

Owen, R. M., and A. M. Olivarez (1988), Geochemistry of rare earth elements in Pacific hydrothermal sediments, *Mar. Chem.*, *25*(2), 183–196, doi:10.1016/0304-4203(88)90063-1.

Petersen, S., K. Kuhn, T. Kuhn, N. Augustin, R. Hékinian, L. Franz, and C. Borowski (2009), The geological setting of the ultramafic-hosted Logatchev hydrothermal field (14°45′N, Mid-Atlantic Ridge) and its influence on massive sulfide formation, *Lithos*, *112*(1–2), 40–56, doi:10.1016/j.lithos.2009.02.008.

Piepgras, D. J., and G. J. Wasserburg (1985), Strontium and neodymium isotopes in hot springs on the East Pacific Rise and Guaymas basin, *Earth Planet. Sci. Lett.*, *72*(4), 341–356, doi:10.1016/0012-821X(85)90057-3.

Rimskaya-Korsakova, M. N., and A. V. Dubinin (2003), Rare earth elements in sulfides of submarine hydrothermal vents of the Atlantic Ocean, *Dokl. Earth Sci.*, *389A*, 432–436.

Rosman, J. R., and P. D. Taylor (1998), Isotopic compositions of the elements (technical report), *Pure Appl. Chem.*, *70*(1), 217–235.

Rouxel, O., Y. Fouquet, and J. N. Ludden (2004), Copper isotope systematics of the Lucky strike, rainbow, and Logatchev sea-floor hydrothermal fields on the Mid-Atlantic Ridge, *Econ. Geol.*, *99*(3), 585–600, doi:10.2113/gsecongeo.99.3.585.

Ruhlin, D. E., and R. M. Owen (1986), The rare earth element geochemistry of hydrothermal sediments from the East Pacific Rise: Examination of a seawater scavenging mechanism, *Geochim. Cosmochim. Acta*, *50*(3), 393–400, doi:10.1016/0016-7037(86)90192-4.

Schade, J., D. H. Cornell, and H. F. J. Theart (1989), Rare earth element and isotopic evidence for the genesis of the Prieska massive sulfide deposit, South Africa, *Econ. Geol.*, *84*(1), 49–63, doi:10.2113/gsecongeo.84.1.49.

Schmidt, K., A. Koschinsky, D. Garbeschonberg, L. Decarvalho, and R. Seifert (2007), Geochemistry of hydrothermal fluids from the ultramafic-hosted Logatchev hydrothermal field, 15°N on the Mid-Atlantic Ridge: Temporal and spatial investigation, *Chem. Geol.*, *242*(1–2), 1–21, doi:10.1016/j.chemgeo.2007.01.023.

Schmidt, K., D. Garbe-Schnberg, M. Bau, and A. Koschinsky (2010), Rare earth element distribution in >400°C hot hydrothermal fluids from 5°S, MAR, the role of anhydrite in controlling highly variable distribution patterns, *Geochim. Cosmochim. Acta*, *63*, 627–643.

Sherrell, R. M., M. P. Field, and G. Ravizza (1999), Uptake and fractionation of rare earth elements on hydrothermal plume particles at 9°45′N, East Pacific Rise, *Geochim. Cosmochim. Acta*, *63*(11–12), 1709–1722, doi:10.1016/s0016-7037(99)00182-9.

Sun, S.-S., and W. F. McDonough (1989), Chemical and isotopic systematics of oceanic basalts: Implications for mantle composition and processes, *Geol. Soc. Spec. Publ.*, *42*, 313–345, doi:10.1144/GSL.SP.1989.042.01.19.

Sun, W., V. C. Bennett, S. M. Eggins, R. J. Arculus, and M. R. Perfit (2003), Rhenium systematics in submarine MORB and back-arc basin glasses: Laser ablation ICP-MS results, *Chem. Geol.*, *196*(1–4), 259–281, doi:10.1016/S0009-2541(02)00416-3.

Sverjensky, D. A. (1984), Europium redox equilibria in aqueous solution, *Earth Planet. Sci. Lett.*, *67*(1), 70–78, doi:10.1016/0012-821X(84)90039-6.

Turekian, K. K. (1968), *Oceans*, Prentice Hall, Engelwood Cliffs, N. J.

Wood, S. A., and A. E. Williams-Jones (1994), The aqueous geochemistry of the rare-earth elements and yttrium 4. Monazite solubility and REE mobility in exhalative massive sulfide-depositing environments, *Chem. Geol.*, *115*(1–2), 47–60, doi:10.1016/0009-2541(94)90144-9.

Yin, X. B., Z. G. Zeng, S. Z. Li, L. Wu, X. Y. Wang, G. L. Zhang, and S. Chen (2011), Determination of trace elements in sulfide samples by inductively coupled plasma-mass spectrometry, *Chin. J. Anal. Chem.*, *39*, 1228–1232.

Zeng, Z., C. Liu, C. A. Chen, X. Yin, D. Chen, X. Wang, X. Wang, and G. Zhang (2007), Origin of a native sulfur chimney in the Kueishantao hydrothermal field, offshore northeast Taiwan, *Sci. China Ser. D*, *50*(11), 1746–1753, doi:10.1007/s11430-007-0092-y.

Zeng, Z., S. Yu, X. Yin, X. Wang, G. Zhang, X. Wang, and D. Chen (2009), Element enrichment and U-series isotopic characteristics of the hydrothermal sulfides at jade site in the Okinawa trough, *Sci. China Ser. D*, *52*(7), 913–924, doi:10.1007/s11430-009-0107-y.

Zeng, Z., D. Chen, X. Yin, X. Wang, G. Zhang, and X. Wang (2010), Elemental and isotopic compositions of the hydrothermal sulfide on the East Pacific Rise near 13°N, *Sci. China Ser. D*, *53*(2), 253–266, doi:10.1007/s11430-010-0013-3.

Zeng, Z., C. A. Chen, X. Yin, X. Zhang, X. Wang, G. Zhang, X. Wang, and D. Chen (2011), Origin of native sulfur ball from the Kueishantao hydrothermal field offshore northeast Taiwan: Evidence from trace and rare earth element composition, *J. Asian Earth Sci.*, *40*(2), 661–671, doi:10.1016/j.jseaes.2010.10.019.

Zeng, Z., S. Chen, D. Selby, X. Yin, and X. Wang (2014), Rhenium–osmium abundance and isotopic compositions of massive sulfides from modern deep-sea hydrothermal systems: Implications for vent associated ore forming processes, *Earth Planet. Sci. Lett.*, *396*, 223–234. doi:10.1016/j.epsl.2014.04.017.